Journal of Statistical Physics, Vol. 107, Nos. 1/2, April 2002 (© 2002)

Development of a Simulation Model for Solid Objects Suspended in a Fluctuating Fluid

Yasuhiro Inoue,[1] Yu Chen,[1] and Hirotada Ohashi[1]

Received February 21, 2001; accepted November 5, 2001

We introduce a new scheme for the future application of Real-coded Lattice Gas (RLG) to the numerical simulation of suspended solid objects in a fluctuating fluid environment. The reproduction of Brownian motion for a single solid object is verified through the Gaussian distribution of its displacements. The effectiveness of the solid–solid interaction model is also confirmed in an *N*-body simulation.

KEY WORDS: Fluctuation phenomena; Brownian motion; solid–liquid flow; lattice gas.

1. INTRODUCTION

A series of discrete mesoscopic fluid models, which include lattice gas automata (LGA),[1] the lattice Boltzmann method (LBM)[2, 3] and dissipative particle dynamics (DPD),[4] have been introduced during the past decade for the analysis of complex fluids. Characteristics of these models in common can be summarized as follows: The detailed microscopic description of fluids has been greatly simplified from the viewpoint of molecular dynamics (MD), though the essential properties to ensure the conservation of mass, momentum and energy (only in some extended models[5, 6]) are preserved without a compromise. On the other hand, the collective or coarse-grained dynamics of the underlying particles approaches the continuum mechanics of real fluids. The reason why these fluid models are appealing lies in several aspects. First, comparing with those conventional numerical methods for flow simulation, such as the finite-difference or the

[1] Department of Quantum Engineering & Systems Science, Graduate school of Engineering, University of Tokyo, 7-3-1 Hongo, Bunkyo-ku, Tokyo 113-8656, Japan; e-mails: inoue@crimson.q.t.u-tokyo.ac.jp, chen@crimson.q.t.u-tokyo.ac.jp, ohashi@crimson.q.t.u-tokyo.ac.jp

0022-4715/02/0400-0085/0 © 2002 Plenum Publishing Corporation

finite-element solution of Navier–Stokes equations, particle-based methods (LGA and DPD) are free from numerical instability. Next, comparing with the more robust microscopic models, such as MD and DSMC (for direct simulation Monte Carlo) these methods are more practical in terms of their computational cost. Note that a very wide spectrum of time and length scales would, in general, characterize the behavior of complex fluids, a fact which requires a higher resolution as well as a longer time progression for the numerical simulation. Third, pattern formation and dynamic flow of complex fluids are often much easier to be modeled in a universal way by intuitively introducing particle interactions or particle structures, rather than trying to establish constitutive relationships from a huge experimental database, in a framework of PDE (for partial differential equations) description for the macroscopic quantities.

Recently, a new mesoscopic model was suggested by Malevanets and Kapral.[7, 8] This model resembles LGA in synchronous discrete time evolution and in discretizing space with regular lattices. On the other hand, positions and velocities of particles are treated as continuous variables. Hence we name the model real-coded lattice-gas (RLG). Other differences between RLG and LGA are the abandonment of exclusion law on particle residence and the use of a stochastic rotational rule for particle interactions. Particle dynamics consists of two processes, namely, streaming and collision. The position of every particle is renewed in the streaming process, and the update of velocity is done in the collision process. Since there is no longer an exclusion law, an arbitrary number of particles can enter into a single cell and multi-particle collisions are carried out there by rotating the relative velocity (to the averaged velocity over the cell) of every particle with a random angle. The kinetic theory of such a particle dynamics tells us that the equilibrium velocity distribution function is Maxwell–Boltzmann and that the existence of an H-theorem can be proved. Furthermore, a set of Galilean-invariant hydrodynamic equations including the transport equation for internal energy can be derived using the Chapman–Enskog expansion. Also, the extension to three-dimensional models can be done in a straightforward way. All these conclusions from previous studies seem very encouraging, as most of the peculiarities of LGA are cured in this model. There is also numerical evidence showing that RLG is computationally more efficient than LGA or DPD. Regarding RLG's advantage over LBM, one may mention the absolute numerical stability and the reproduction of fluctuating hydrodynamics, the latter of which would be very useful, for example, in studying problems with flow instability or the Brownian motions.

Although research on RLG is still in its infancy and fundamental questions of the model, such as the expression of transport coefficients, the

validity of molecular chaos and the proof for Galilean invariance, are to be clarified,[9] various applications have already been challenged in simulations of complex fluids: the solvent dynamics,[10] the dynamics of short polymer chains,[11] the extension to immiscible two-phase models,[12] the amphiphilic surfactant models,[13,14] and the simulation of a single rising bubble.[15] In this study, we shall introduce a new scheme for the future application of RLG to suspended solid objects in a fluctuating fluid environment. A large number of documents on direct numerical simulation of solid–liquid flow using the conventional Navier–Stokes solver can be found from the web site (provided by D. D. Joseph): http://www.aem.umn.edu/Solid-Liquid_Flows. On the other hand, the same kind of work has been done with the use of these mesoscopic fluid models (mainly LBM models[16–18]), all of which showed impressive agreement with experiments and the mainstream studies. The goal for this study is, however, not as ambitious as to compare in detail with those results or to present new results in this field (these are planed for future studies). We shall concentrate on the introduction of the necessary techniques to perform such a simulation with the RLG model.

The outline of this paper is as follows. Section 2 outlines the RLG model and shows the conservation of mass, momentum and energy. The reflection of RLG particles on the surface of a solid object, as well as the solid–solid interactions will be detailed in Section 3. In Section 4, numerical simulations will be displayed as demos of the suggested model. The concluding remarks will be made in Section 5.

2. A BRIEF SUMMARY OF THE RLG MODEL

First of all, it might be helpful to give an explanation of the relation between the original "continuous velocity lattice-gas" model[7,8] and the current RLG model. In the previous publication,[7] Malevanets and Kapral employed a stochastic method for the complete translation of each particle in the simulation system. In particular, each particle is translated accurately only according to the integer part of its velocity. The fractional part of its velocity is used, however, as a probability distribution for a random walk process that followed. The consequence of this special translation is that particles can meet others at a lattice site (the crossing point of lattice links). Therefore the "physical contacts" of particles are ensured in the pre-collision stage. In fact, the random walk process could be unnecessary for two reasons: first, collisions can occur among particles staying in a single cell instead of at a single site; Second, since particles are distributed uniformly within a single cell, translating particles accurately (according to both the

integer and fractional part of coordinates) is equivalent to translating them from the randomly shifted locations (with integer coordinates).

We realized these facts and converted the original model to RLG. Note that Malvanets and Kapral also developed the same idea independently at almost the same time.[8] The computational efficiency of RLG is improved without the random walk process. Nevertheless, the effects of numerical viscosity still exist in both the models. In the continuous velocity lattice-gas, the numerical viscosity is explicitly added through the random walk process. In the RLG model, however, the diffusion of velocities can not be avoided because of the exchange of momenta among distant particles. The investigation of influences of cell size and cell shape to the numerical dissipation of RLG is an important topic which has not been studied yet.

The kernel of RLG consists of two processes. One is the particle-streaming process, in which the position vectors of RLG particles would be incremented by their displacements through a unit time, namely,

$$\mathbf{x}_i(t+1) = \mathbf{x}_i(t) + \mathbf{v}_i(t) \tag{1}$$

Here $\mathbf{x}_i(t)$ is the location and $\mathbf{v}_i(t)$ is the velocity of the ith particle at time t, respectively. The other process is collision, during which RLG particles exchange their momentum and kinetic energy if they happened to reside in the same collision cell, with the following algorithm,

$$\mathbf{v}_i(t+1) = \mathbf{V} + \mathbf{\Omega}(\mathbf{v}_i(t) - \mathbf{V}) \tag{2}$$

The rotation operation $\mathbf{\Omega}$ can be written explicitly, for example in 2D space with an arbitrary deflection θ as follows,

$$\mathbf{\Omega} = \begin{pmatrix} \cos\theta & -\sin\theta \\ \sin\theta & \cos\theta \end{pmatrix} \tag{3}$$

Here $\mathbf{V}$ is the velocity of the center of mass of those "colliding particles." Usually a square lattice with links of unit length is employed in RLG, so that the shape of a single collision cell is square in 2D or cubic in 3D. Consider the center of such a cell is located at $\mathbf{x} = \sum_{\mathrm{m}=1}^{D} (\mathbf{r} \cdot \mathbf{e}_m + \frac{1}{2})\, \mathbf{e}_m$ where $\mathbf{r}$ denotes the arbitrary lattice point vector and $\mathbf{e}_m$ indicates the unit vector along the m axis. If the mass of the ith particle is denoted as m_i, $\mathbf{V}$ can be calculated as

$$\mathbf{V}(\mathbf{x}, t) = \frac{1}{M(\mathbf{x}, t)} \sum_{i \in \{j;\, [\mathbf{x}_j] = [\mathbf{x}]\}} m_i \mathbf{v}_i(t) \tag{4}$$

where $M(\mathbf{x}, t)$ is the total mass of particles in the cell and $[\mathbf{x}]$ is the integer part of $\mathbf{x}$. In the following text, the summation operator will be written as $\sum_{i;\mathbf{x}}$ for simplicity. Obviously, the total mass is defined with the summation operator as follows.

$$M(\mathbf{x}, t) = \sum_{i;\mathbf{x}} m_i \tag{5}$$

The collision matrix $\boldsymbol{\Omega}$ can be selected randomly from the rotation group which can ensure the conservation of mass, momentum and energy. In practice, the rotation angle is chosen as $\theta = \pm\frac{\pi}{2}$, which has been suggested[7] as a good way to achieve a lower viscosity as long as the mean free path is long compared to the cell size.[9] The conservation of momentum $\mathbf{Q}(\mathbf{x}, t) = \sum_{i;\mathbf{x}} m_i \mathbf{v}_i$ before and after the multi-particle collision can be easily shown as follows:

$$\begin{aligned}
\sum_{i;\mathbf{x}} m_i \mathbf{v}_i(t+1) &= \sum_{i;\mathbf{x}} m_i \mathbf{V}(\mathbf{x}, t) + \sum_{i;\mathbf{x}} m_i \boldsymbol{\Omega}(\mathbf{v}_i(t) - \mathbf{V}(\mathbf{x}, t)) \\
&= \sum_{i;\mathbf{x}} m_i \mathbf{v}_i(t) + \boldsymbol{\Omega} \sum_{i;\mathbf{x}} m_i (\mathbf{v}_i(t) - \mathbf{V}(\mathbf{x}, t)) \\
&= \sum_{i;\mathbf{x}} m_i \mathbf{v}_i(t)
\end{aligned} \tag{6}$$

where the relation $\sum_{i;\mathbf{x}} m_i(\mathbf{v}_i(t) - \mathbf{V}(\mathbf{x}, t)) = 0$ is used here. The conservation of the total energy $E(\mathbf{x}, t) = \sum_{i;\mathbf{x}} \frac{1}{2} m_i \mathbf{v}_i^2(t)$ can be also proved as follows.

$$\begin{aligned}
&\sum_{i;\mathbf{x}} \tfrac{1}{2} m_i \mathbf{v}_i^2(t+1) \\
&\quad = \sum_{i;\mathbf{x}} \tfrac{1}{2} m_i \{\mathbf{V}(\mathbf{x}, t) + \boldsymbol{\Omega}(\mathbf{v}_i(t) - \mathbf{V}(\mathbf{x}, t))\}^{\mathrm{T}} \{\mathbf{V} + \boldsymbol{\Omega}(\mathbf{v}_i(t) - \mathbf{V}(\mathbf{x}, t))\} \\
&\quad = \sum_{i;\mathbf{x}} \tfrac{1}{2} m_i \{\mathbf{V}^{\mathrm{T}}\mathbf{V} + (\mathbf{v}_i - \mathbf{V})^{\mathrm{T}} \boldsymbol{\Omega}^{\mathrm{T}} \boldsymbol{\Omega} (\mathbf{v}_i - \mathbf{V})\} \\
&\quad = \sum_{i;\mathbf{x}} \tfrac{1}{2} m_i (\mathbf{V}^{\mathrm{T}}\mathbf{V} + \mathbf{v}_i^{\mathrm{T}}\mathbf{v}_i - \mathbf{V}^{\mathrm{T}}\mathbf{V} - \mathbf{V}^{\mathrm{T}}\mathbf{V} + \mathbf{V}^{\mathrm{T}}\mathbf{V}) \\
&\quad = \sum_{i;\mathbf{x}} \tfrac{1}{2} m_i \mathbf{v}_i^2(t)
\end{aligned} \tag{7}$$

Here, the superscript T means the transpose of a matrix or a vector. The fact that the rotation matrix is orthogonal ($\boldsymbol{\Omega}^{\mathrm{T}}\boldsymbol{\Omega} = \mathbf{1}$) and the definition of $\mathbf{V}$ are used in the proof above. The velocity distribution for RLG particles

will become that of Maxwell–Boltzmann if the two processes are executed till the whole system reaches the equilibrium state. Macroscopic variables of the fluid model are obtained from the ensemble averages of the summed quantities. In particular, the fluid density is calculated by $\rho(\mathbf{x}, t) = \langle M(\mathbf{x}, t) \rangle$, the flow velocity by $\mathbf{v}(\mathbf{x}, t) = \langle \mathbf{V}(\mathbf{x}, t) \rangle$, and the temperature by $T(\mathbf{x}, t) = \langle E(\mathbf{x}, t) - \frac{1}{2} M(\mathbf{x}, t)\, \mathbf{V}^2(\mathbf{x}, t) \rangle / C_v$, where $C_v = d/2$ is the specific heat of the $d-$dimensional model. It was proved that these variables obey the hydrodynamic equations for an ideal gas.[8]

3. MODELLING OF THE SUSPENDED SOLID OBJECTS

3.1. The Interaction Between RLG Particles and a Solid Object

In our simulation model, the fluctuating fluid phase is described by RLG particles, while each solid object is considered as being composed of a finite number of solid particles. The function of these solid particles which stick firmly to each other is to express any possible shapes for the whole solid object. Although solid particles constrained in this way can not play any active roles in the scheme, they will be useful for the future development of the model (we shall eventually allow and formulate the relative motions of these particles to take the deformations of solid objects into account). At the current stage, the statement that solid objects and RLG particles are exclusive to each other is enough to determine the interaction between them.

3.1.1. The Detection of Reflections

When RLG particles collide with a solid object, they are reflected according to principles of Newtonian mechanics. Before we describe the way in which RLG particles are reflected, a simple method for the detection of such collisions is suggested and described in reference with Fig. 1.

First step, we pick up those solid particles residing on the surface of the solid object and define them as "surface tracers;" see Fig. 1(a). In the second step, the interacting area is determined according to the surface tracers' positions and the normal vectors. In particular, it is formed by cells, where the surface tracers locate, and their neighbors inside the solid object. Finally, every RLG particle residing in an interacting cell is marked with a flag for reflection according to the scalar product of the normal vector $\mathbf{n}$ of the solid surface and the vector representing the relative position to the local surface tracer. For example, the flag of particles A in Fig. 1(c) is `OFF`, that is, it will not be reflected. On the other hand, the flag of particle B in the same figure is `ON`, because the scalar product $(\vec{OB} \cdot \mathbf{n})$ is

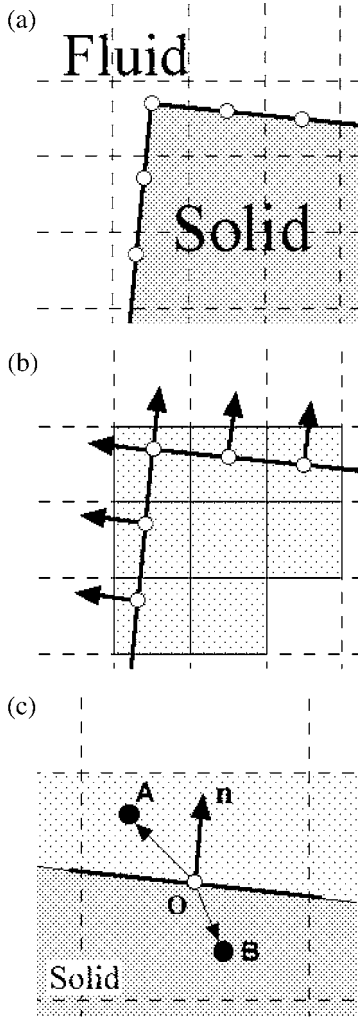

Fig. 1. The detection of collision between RLG particles and a solid object. In these figures, transparent circles stand for surface tracers, which are defined as solid particles residing on the surface of the solid object. Solid circles represent RLG particles. Thick arrows indicate the normal vector of the local surface and thin arrows indicate the relative position of RLG particles to the surface tracer. Gray area are the internal region of the solid object. Cells of light gray color form the interacting area, in which every RLG particle will be checked to see if the reflection scheme should be applied.

negative. The reflection of RLG particles are completed according to schemes introduced in the following section.

3.1.2. The Reflection of RLG Particles

Reflections of RLG particles on the surface of a solid object are considered to be elastic ones. Specifically, the velocity of a RLG particle is abandoned and a new velocity after the reflection is generated randomly according to the following probability density distributions (PDFs).

$$P_n(c_n) = m\beta c_n \exp\left(-\beta \frac{1}{2} m c_n^2\right) \tag{8}$$

$$P_t(c_t) = \sqrt{\frac{m\beta}{2\pi}} \exp\left(-\beta \frac{1}{2} m c_t^2\right) \tag{9}$$

Here the subscripts n and t represent the normal and the tangential directions of the solid surface. The mass of each RLG particle is assumed to be universal and indicated by m. The velocity $\mathbf{c}$ stands for the velocity of RLG particles observed from a moving coordinate that is fixed on the solid object. The temperature $T = 1/\beta$ is equivalent to the temperature of the solid object. The PDF for the tangential velocity components is simply Maxwellian and both positive and negative values are acceptable. For the normal velocity components, however, only the positive values are adopted to ensure the exclusion principle between RLG particles and solid objects. The derivation of PDF for the normal velocities is shown in the following text.

Consider an imaginary plane of a unit area moving along the z-axis (the normal direction of the plane) in an ideal gas system which is assumed to be in the thermal equilibrium state. Then how many particles can go through this plane along the z direction in a unit time? Using the fact that the velocity distribution of particles is Maxwellian, we may calculate the number of these particles as follows.

$$N_z^0 = \int_{-c_z}^{0} dz \iint_{-\infty}^{+\infty} dc_x\, dc_y \int_0^{+\infty} dc_z \frac{N}{V} \left(\sqrt{\frac{m\beta}{2\pi}}\right)^3 \exp\left(-\beta \frac{1}{2} m\mathbf{c}^2\right)$$

$$= \frac{N}{V\sqrt{2\pi m\beta}} \tag{10}$$

Here, N and V are the total particle number and the volume of the ideal gas. The relative velocities of particles are again denoted as vector $\mathbf{c}$. Next,

we consider the number of particles going through the surface whose z-component of velocity is between c_z and $c_z + \Delta c_z$.

$$N_z(c_z) = \int_{-c'_z}^{0} dz \iint_{-\infty}^{+\infty} dc'_x\, dc'_y \int_{c_z}^{c_z+\Delta c_z} dc'_z \frac{N}{V}\left(\sqrt{\frac{m\beta}{2\pi}}\right)^3 \exp\left(-\beta\frac{1}{2}m\mathbf{c}'^2\right)$$

$$= \frac{N}{V}\sqrt{\frac{m\beta}{2\pi}}\left[-\frac{1}{m\beta}\exp(-\beta\frac{1}{2}mc'^2_z)\right]_{c_z}^{c_z+\Delta c_z}$$

To proceed the calculation, we use the Taylor expansion as follows.

$$N_z(c_z) = \frac{N}{V}\sqrt{\frac{m\beta}{2\pi}}\left\{c_z \exp\left(-\beta\frac{1}{2}mc_z^2\right)\Delta c_z\right.$$

$$\left. + \frac{1}{2}\left(\exp\left(-\beta\frac{1}{2}mc_z^2\right) - m\beta c_z^2 \exp\left(-\beta\frac{1}{2}mc_z^2\right)\right)(\Delta c_z)^2 + \cdots\right\}$$

$$\simeq \frac{N}{V}\sqrt{\frac{m\beta}{2\pi}}\, c_z \exp\left(-\beta\frac{1}{2}mc_z^2\right)\Delta c_z \tag{11}$$

The ratio of the two numbers, namely, N_z/N_z^0 can be used to calculate the PDF of these particles,

$$P(c_z)\, dc_z \equiv \frac{N(c_z)}{N_z^0}$$

$$= m\beta c_z \exp\left(-\beta\frac{1}{2}mc_z^2\right) dc_z \tag{12}$$

To justify the use of this PDF as the normal velocity distribution for the RLG particles which are reflected elastically on the solid surface, the solid object has to be regarded as a heat bath, which seems to be a reasonable argument.

Through the reflections of RLG particles, an amount of $\Delta\mathbf{Q}$ of translational momentum is exchanged, meanwhile an amount of $\Delta\mathbf{L}$ of angular momentum will contribute to the motion of the solid object. These quantities can be calculated as follows.

$$\Delta\mathbf{Q} = \sum_{i;\,\text{reflected}} (\mathbf{v}'_i - \mathbf{v}_i)\, m_i \tag{13}$$

$$\Delta\mathbf{L} = \sum_{i;\,\text{reflected}} \mathbf{r}_s \times (\mathbf{v}'_i - \mathbf{v}_i)\, m_i \tag{14}$$

Here $\mathbf{v}_i'$ indicates the particle velocity after the reflection and $\mathbf{r}_s$ represents the distance between the colliding position of the ith RLG particle, namely, the position of the local surface tracer, and the center of mass of the solid object. Finally, the motion of solid object is determined by increments of the translational momentum and angular momentum, respectively.

$$\mathbf{Q}'_{\text{object}}(t+\Delta t_f) = \mathbf{Q}_{\text{object}} + (-\Delta \mathbf{Q}) \tag{15}$$

$$\mathbf{L}'_{\text{object}}(t+\Delta t_f) = \mathbf{L}_{\text{object}} + (-\Delta \mathbf{L}) \tag{16}$$

For the calculation of these interactions, a smaller time step ($\Delta t_f < 1$) is employed.

3.2. Motions and Interactions of Solid Objects

Motions of solid object consist of a translational one and a rotational one according to their translational and angular velocities. If a solid object encounters another one, they would collide with each other. The solid–solid interaction can be modeled through a colliding impulse P.

A fourth order Runge-Kutta method is employed for the time integration of solid objects' motions, because the rotation of every solid object need to be calculated with a higher accuracy. To ensure the numerical stability for the Runge-Kutta method, we choose a much smaller time step $\Delta t_s \ll \Delta t_f \ll 1$. Furthermore, it would be computationally expensive if we let solid objects move simultaneously. For, multiple objects can easily overlap with each other through their motions. If this had happened, we would have to go back and do the calculation again with a smaller time step. To avoid the use of an adaptive time step for the solid objects' motion, we use a random order list for the time evolution. Every solid object is moved according to the order list. If two solid particles are found in the same cell, the solid–solid interaction will be disposed with priority.

Next, we show the derivation of the colliding impulse P for an interaction between two solid objects. The colliding impulse is defined[19] as $P\mathbf{n} = \int_{\Delta t} \mathbf{F}(t)\, dt$, where $\mathbf{F}(t)$ is the colliding force acting on the solid objects. During the solid–solid interaction, the translational velocities $(\mathbf{U}_1, \mathbf{U}_2)$ and the angular velocities $(\boldsymbol{\omega}_1, \boldsymbol{\omega}_2)$ will be renewed as $(\mathbf{U}_1', \mathbf{U}_2')$ and $(\boldsymbol{\omega}_1', \boldsymbol{\omega}_2')$, namely,

$$\mathbf{U}_1' = \mathbf{U}_1 + P\mathbf{n}/M_1, \qquad \boldsymbol{\omega}_1' = \boldsymbol{\omega}_1 + \mathbf{I}_1^{-1}(\mathbf{r}_1 \times \mathbf{n}P) \tag{17}$$

$$\mathbf{U}_2' = \mathbf{U}_2 - P\mathbf{n}/M_2, \qquad \boldsymbol{\omega}_2' = \boldsymbol{\omega}_2 - \mathbf{I}_2^{-1}(\mathbf{r}_2 \times \mathbf{n}P) \tag{18}$$

where M_1 and M_2 are the mass, $\mathbf{I}_1$ and $\mathbf{I}_2$ are the moment of inertia of the two colliding objects. Vectors $\mathbf{r}_1$ and $\mathbf{r}_2$ connect to the center of mass of

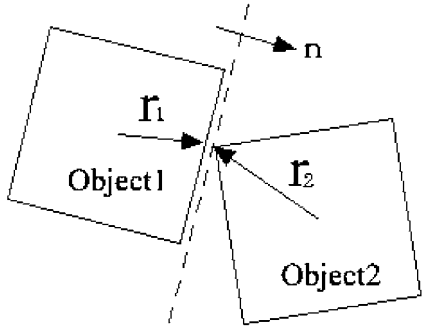

Fig. 2. Vectors $\mathbf{r}_1$ and $\mathbf{r}_2$ connect the colliding point to the center of mass of each object. In this case, object 1 would actively encounter object 2, because it happened to be at a prior position in the random list for the time evolution. Here the normal vector $\mathbf{n}$ of the collision surface is defined as the normal vector of the surface of object 1.

each object to the colliding point, see Fig. 2. The normal vector of the colliding surface $\mathbf{n}$ is specified in the caption of the same figure. We consider only the velocity difference between the initial and the final state of the collision.

$$(\mathbf{u}_1' - \mathbf{u}_2') - (\mathbf{u}_1 - \mathbf{u}_2) = \frac{P\mathbf{n}}{M_1} + \{\mathbf{I}_1^{-1}(\mathbf{r}_1 \times \mathbf{n}P)\} \times \mathbf{r}_1 + \frac{P\mathbf{n}}{M_2} + \{\mathbf{I}_2^{-1}(\mathbf{r}_2 \times \mathbf{n}P)\} \times \mathbf{r}_2 \tag{19}$$

where $\mathbf{u}_i = \mathbf{U}_i + \boldsymbol{\omega} \times \mathbf{r}_i$, $i = 1, 2$. We apply the Newton's impact law along the normal axis of the collision surface, namely,

$$\frac{(\mathbf{u}_1' - \mathbf{u}_2') \cdot \mathbf{n}}{(\mathbf{u}_1 - \mathbf{u}_2) \cdot \mathbf{n}} = -e \tag{20}$$

Using the scalar product of Eq. (19) and $\mathbf{n}$, we can obtain the expression for the colliding impulse.

$$P = \frac{-(1+e)(\mathbf{u}_1 - \mathbf{u}_2) \cdot \mathbf{n}}{\{(1/M_1 + 1/M_2)\,\mathbf{n} + (\mathbf{I}_1^{-1}(\mathbf{r}_1 \times \mathbf{n})) \times \mathbf{r}_1 + (\mathbf{I}_2^{-1}(\mathbf{r}_2 \times \mathbf{n})) \times \mathbf{r}_2\} \cdot \mathbf{n}} \tag{21}$$

Once we know the colliding impulse, translational and angular velocities of the solid object can be calculated using Eqs. (17) and (18).

4. SIMULATION OF THE BROWNIAN MOTION

We carried out two numerical simulations to show the effectiveness of the model. The first simulation is for a single object in a fluctuating fluid.

In this case, we show that displacements of the object follow a Gaussian distribution. The second simulation is concerned with a N-body simulation, where we want to check the solid–solid collision model. In both the simulations, the mean density of RLG particles is set to 5. This number density can ensure a correct hydrodynamics for RLG fluid. If the number density is much less than 1, the mean free path of RLG particles could become longer than the solid object length, a condition that hydrodynamics would break down. On the other hand, a much higher density would certainly reduce the noise of physical quantities at every time step. It simply becomes too expensive to do the calculation. Thus we average hydrodynamic quantities over a long enough time period after the simulation enters into the steady state. This means that the time-averaged quantities are regarded as the mean values in the canonical ensemble.

4.1. Simulation of a Single Solid Object

The solid object is a 12×12 square and composed by 144 solid particles. The mass of each solid particle is 1 which is equivalent to that of each RLG particle. However the mean density of a solid object is much less than that of the RLG fluid, which has been set to 5. The background fluid is statistically isotropic and stationary, namely the mean flow velocity is zero. The temperature of the system is set to 0.5 so that the solid object motion can be driven by the fluctuation in the background fluid, that is, the bombardment of RLG particles on its surface. The basic noise of RLG model has been numerically proven to be physical in a hybrid MD simulation of solute-solvent dynamics.[10] In this simulation, we measured displacements of the solid object as a function of the elapsed time τ. In particular, the displacement of the solid object is calculated by

$$\Delta\mathbf{X}_\tau(t) = \mathbf{X}(t) - \mathbf{X}(t-\tau)$$

where $\mathbf{X}(t)$ indicate the position vector for the center of mass of a solid object at time t. And we measured these displacements from 20000 steps to 40000 steps at every $\tau = 1/10$. Here totally 200000 samples were obtained and we think that this is good enough number to obtain a smooth probability distribution function for the solid displacements. It is well known that the probability distribution for such displacements would be Gaussian when the relaxation time for the decay of autocorrelation in the momentum of the solid object is much shorter than the time for observation. This also demonstrates that the solid object is really doing the Brownian motion. The results for the case $\tau = 1/10$ over a 20000-step period are shown in Fig. 3,

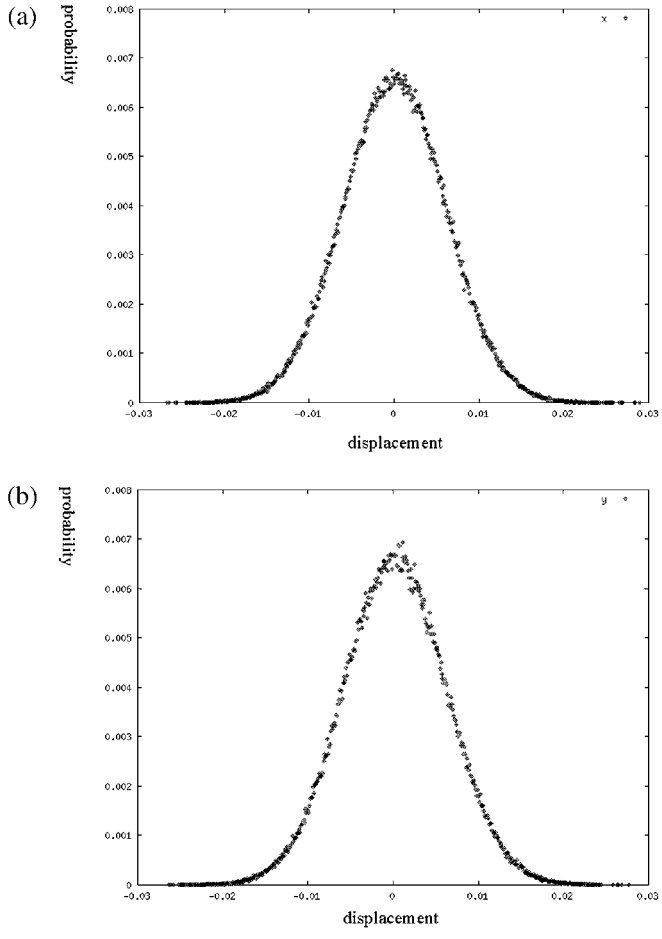

Fig. 3. 2D simulation of a single solid object doing Brownian motion in the background fluid. The Gaussian distributions of displacements in the x and y directions reflect the nature of such a fluctuating phenomenon. (a) Displacements in the x direction; (b) displacements in the y direction.

where one can easily find that the probability distribution for displacements is Gaussian as expected.

4.2. *N*-Body Simulation

The shape of each solid object is a 6×6 square in this numerical experiment. There are 20 solid objects, which are suspended in a fluid formed by 18000 RLG particles. The size of the fluid regime is 60×60 with

doubly periodic boundaries. Each solid object is initialized with a zero velocity. The initial velocity of the fluid is also set to zero, however, only in a statistical sense, since a non-zero temperature ($T = 0.5$) is chosen for the system. When the simulation started, these solid objects were naturally driven by RLG particles and began to do the Brownian motion, see Fig. 4. This situation is almost the same as the previous example, except that solid–solid interactions become possible due to the multiple existences of solid objects. We take an example of such interactions from the configuration at $t = 250$ time steps. The details are shown in the Fig. 5 and its caption.

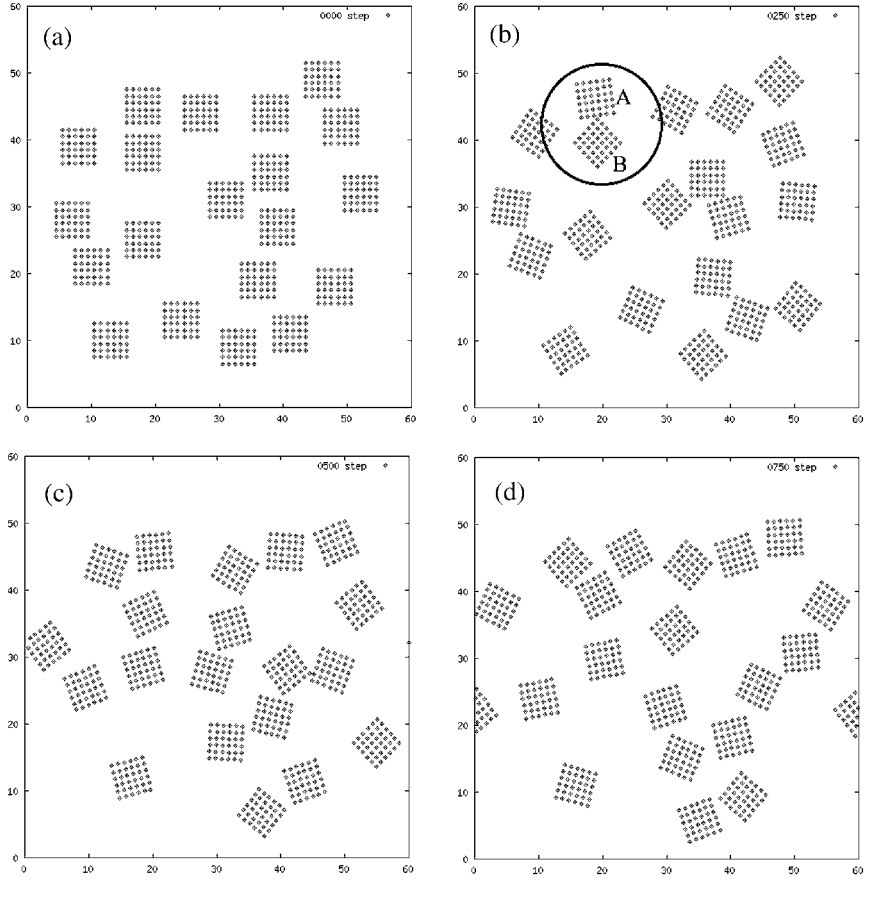

Fig. 4. *N*-Body's Brownian motion in a system with doubly periodic system. (a) $t = 0$; (b) $t = 250$; (c) $t = 500$; (d) $t = 750$. The region highlighted with a circle in (b) indicates a solid–solid interaction between A and B.

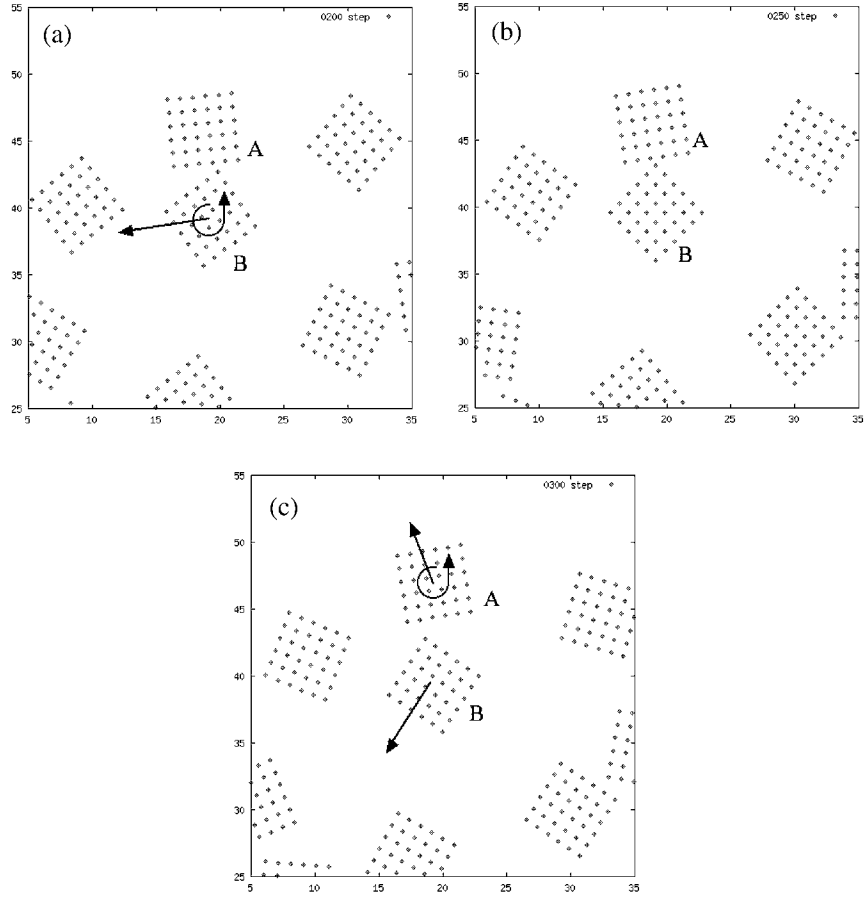

Fig. 5. The solid–solid interaction between object A and object B. Line arrows represent the translational velocities, while the curved arrows represent the rotating direction. (a) At $t = 200$, object A has almost a zero translational velocity and a very small angular velocity. (b) The interaction occurs at $t = 250$. After this interaction, object A has a translational velocity together with and a counter-clock wise angular velocity. (c) $t = 300$.

5. CONCLUSION

We developed a new scheme for the simulation of suspended solid objects in a fluctuating fluid environment. The RLG model is shown to have a huge potential for the simulation of complex flows. Our model is able to deal with both the fluid–solid and the solid–solid interactions. Brownian motions of a single and multiple solid objects are naturally

reproduced in the simulation. In the near future, we will verify the quantitative accuracy of this model through some 3D benchmarks.

REFERENCES

1. U. Frisch, B. Hasslacher, and Y. Pomeau, Lattice-gas automata for the Navier–Stokes equations, *Phys. Rev. Lett.* **56**:1505 (1986).
2. G. R. Mcnamara and G. Zanetti, Use of the Boltzmann equation to simulate lattice-gas automata, *Phys. Rev. Lett.* **61**:2332 (1988).
3. S. Chen and G. D. Doolen, Lattice Boltzmann method for fluid flows, *Ann. Rev. Fluid Mech.* **30**:329 (1998).
4. P. J. Hoogerbrugge and J. M. V. A. Koelman, Simulating microscopic hydrodynamics with dissipative particle dynamics, *Europhys. Lett.* **19**:155 (1992).
5. H. Chen, C. Teixeira, and K. Molvig, Digital physics approach to computational fluid dynamics: Some basic theoretical features, *Mod. Phys. C* **8**:675 (1997).
6. Y. Chen, H. Ohashi, and M. Akiyama, Thermal lattice Bhatnagar–Gross–Krook model without nonlinear deviations in macroscopic equations, *Phys. Rev. E*, **50**:2776 (1994).
7. A. Malevanets and R. Kapral, Continuous-velocity lattice-gas model for fluid flow, *Europhys. Lett.* **44**:552 (1998).
8. A. Malevanets and R. Kapral, Mesoscopic model for solvent dynamics, *J. Chem. Phys.* **10**:8605 (1999).
9. T. Ihle and D. M. Kroll, Stochastic rotation dynamics: A Galilean-invariant mesoscopic model for fluid flow, *Phys. Rev. E* **63**:020201(R) (2001).
10. A. Malevanets and R. Kapral, Solute molecular dynamics in a mesoscale solvent, *J. Chem. Phys.* **12**:7260 (2000).
11. A. Malevanets and J. M. Yeomans, Dynamics of short polymer chains in solution, *Europhys. Lett.* **52**:231 (2000).
12. Y. Hashimoto, Y. Chen, and H. Ohashi, Immiscible real-coded lattice gas, *Comp. Phys. Comm.* **129**:56 (2000).
13. T. Sakai, Y. Chen, and H. Ohashi, Formation of micelle in the real-coded lattice gas, *Comp. Phys. Comm.* **129**:75 (2000).
14. T. Sakai, Y. Chen, and H. Ohashi, A real-coded lattice gas model for ternary amphiphilic fluids. To be published in the same proceedings.
15. Y. Hashimoto, Doctoral thesis, University of Tokyo (2000).
16. A. J. C. Ladd, Short-time motion of colloidal particles: Numerical simulation via a fluctuating lattice-Boltzmann equation, *Phys. Rev. Lett.* **70**:1339 (1993).
17. A. J. C. Ladd, Sedimentation of homogeneous suspensions of non-Brownian spheres, *Phys. Fluids* **9**:491 (1997).
18. C. K. Aidun and Y. N. Lu, Lattice Boltzmann simulation of solid particles suspended in fluid, *J. Stat. Phys.* **81**:49 (1995).
19. H. Goldstein, *Classical Mechanics*, 2nd ed. (Addison–Wesley, 1980).